Eur. Phys. J. A **25**, s01, 757–762 (2005)
DOI: 10.1140/epjad/i2005-06-148-3

EPJ A direct
electronic only

Spallation reactions for nuclear waste transmutation and production of radioactive nuclear beams

J. Benlliure[a]

Universidade de Santiago de Compostela, 15706 Santiago de Compostela, Spain

Received: 12 January 2005 / Revised version: 12 April 2005 /
Published online: 14 July 2005 –

Abstract. Spallation reactions are considered an optimum neutron source for nuclear waste transmutation in accelerator-driven systems (ADS). They are also used to produce intense radioactive nuclear beams in ISOL facilities. A difficulty in both applications is the characterisation of these reactions in terms of residual nuclei production. In this paper we review the GSI experimental program for the investigation of spallation reactions and their implications both in radioactive nuclear beams production and basic nuclear structure research.

PACS. 25.40.Sc Spallation reactions – 21.10.-k Properties of nuclei; nuclear energy levels

1 Introduction

Spallation reactions have been proposed as an optimum neutron source to feed subcritical reactors in accelerator driven systems (ADS) used to burn long-lived nuclear waste [1] or produce energy [2]. These reactions are also considered for the production of intense radioactive nuclear beams using the ISOL technique [3,4]. A common issue in both applications is the design of the spallation targets, which requires making a complete inventory of residual nuclides produced in these reactions.

Until now, most of the available information on residual nuclei production in spallation or fragmentation reactions has been obtained using radiochemical or spectroscopic methods. Unfortunately, these techniques only provide isobaric information on the produced nuclei, and the isotopic production cross sections for only a few shielded nuclides. A few years ago, a new experimental technique based on the combined use of inverse kinematics and a high-resolution magnetic spectrometer was proposed at GSI. This new technique allows for the isotopic identification of all reaction residues.

For the last several years, a large experimental program has been underway at GSI, which uses the abovementioned technique, to measure the isotopic production cross sections and kinematic properties of all residual nuclides produced in spallation reactions. The high-quality data it provides has allowed us to improve our present understanding on this reaction mechanism, to draw some important conclusions about the production of radioactive nuclear beams or to investigate some basic nuclear structure features. In this paper we review some of the highlights of the GSI program.

[a] e-mail: j.benlliure@usc.es

2 Experiments and results

The experiments have been carried out at the SIS synchrotron at GSI (Germany). Primary beams of ^{238}U, ^{208}Pb, ^{197}Au, ^{136}Xe and ^{56}Fe accelerated at energies between 300 and 1000 A MeV impinged on a liquid hydrogen or deuteron target. At these energies all reaction residues are predominantly fully stripped, bare ions. The achromatic high resolution magnetic spectrometer FRS [5] equipped with an energy degrader, two position-sensitive scintillators and a multi-sampling ionisation chamber made it possible to identify the mass and atomic number of all the residual nuclides with half lives longer than 200 ns. This technique provided resolutions of $A/\Delta A \approx 400$ and $Z/\Delta Z \approx 150$, and final production cross sections could be evaluated with near 10% accuracy. The high resolution of the magnetic spectrometer also enabled us to determine the recoil velocity of the reaction residues. This information is relevant both to investigating the nature of the reaction mechanism responsible of the production of the residual nuclei and for characterising radiation-induced damages in the accelerator window or structural materials on an ADS. More details about these experiments can be found in references [6,7,8,9] and a complete set of data in [10].

In fig. 1, all residues measured in the reactions ^{208}Pb(1 A GeV) + p [6,9] and ^{238}U(1 A GeV) + p, d, Ti [11,12,13,14] are presented in form of a chart of the nuclides

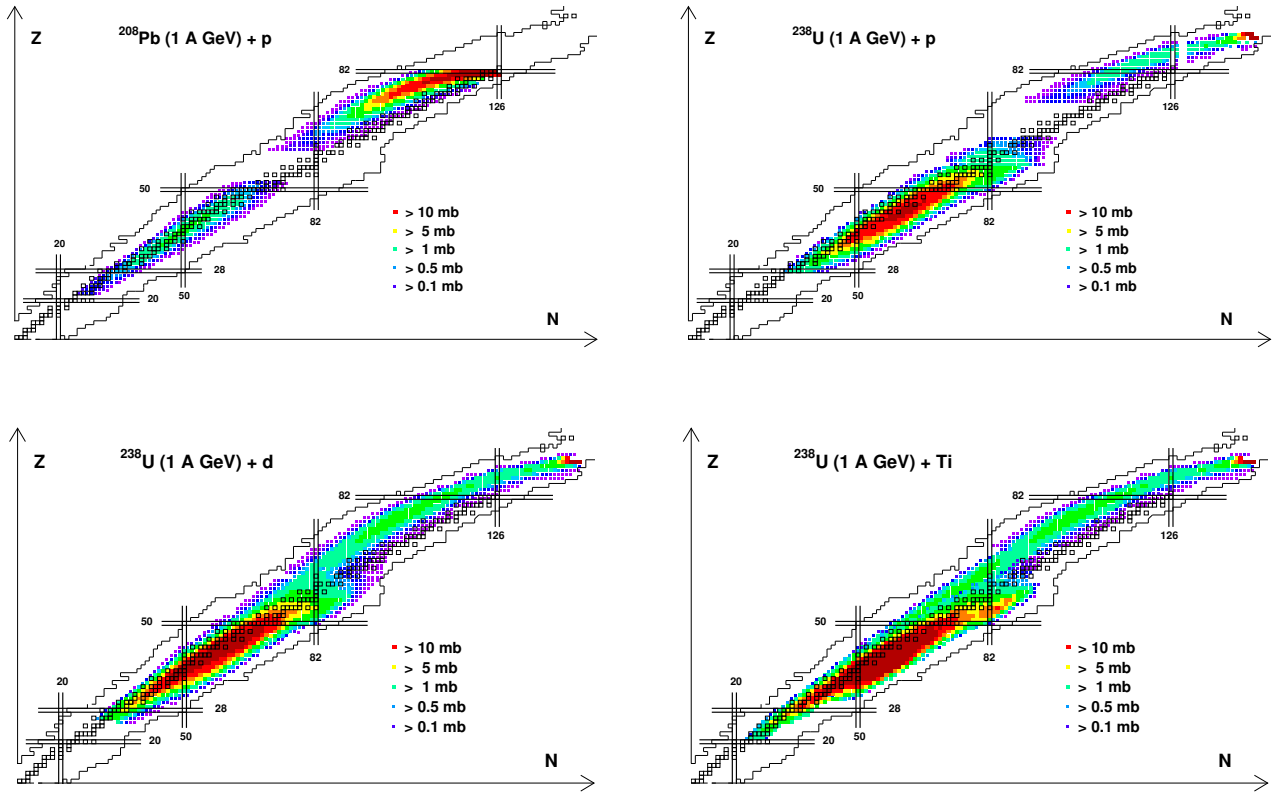

Fig. 1. Two-dimensional cluster plot of the isotopic production cross sections of all the spallation residues measured at GSI in the reactions ^{208}Pb(1 A GeV)+p, ^{238}U(1 A GeV)+p, ^{238}U(1 A GeV)+d and ^{238}U(1 A GeV)+Ti shown on top of a chart of the nuclides.

with a colour code according to five cross sections ranges whose lower limits are indicated. More than 1100 different nuclei were identified in each reaction. Spallation residues populate two different regions of the chart of the nuclides. The high-Z region corresponds to the spallation-evaporation residues which populate the so called evaporation-residue corridor. The low-Z region represents medium-mass residues produced in spallation-fission reactions. Though inherently different, both fission and evaporation contribute to the production of residues.

3 Implications for the production of radioactive nuclear beams

These data are also relevant to understanding the expected yields of exotic beams, with a view to finding the reaction mechanisms best suited to extending the present limits of the nuclide chart. The accuracy of the new data has improved our understanding of these mechanisms and allowed to explore the prospects of producing rare isotopes in different regions of the nuclide chart. In the next sections we present some examples of these investigations.

3.1 Production of heavy neutron-rich nuclei

Recent investigations reveals large fluctuations in the N/Z and excitation-energy distribution of the final residues of fragmentation reactions at relativistic energies. Specifically, proton-removal channels have been investigated in cold-fragmentation reactions [15], where protons only are abraded from the projectile while the induced excitation energy is below the particle-emission threshold. These reactions could produce heavy neutron-rich nuclei beyond the present limits of the chart of the nuclides.

Using the abrasion-ablation model, these reactions can be explained as a two-step process. The interaction between projectile and target leads to a projectile-like residue with a given excitation energy which then statistically de-excites by particle evaporation or by fission. A new analytical formulation of the abrasion-ablation model, the code COFRA [15], has been developed to calculate the expected low production cross sections of extremely neutron-rich nuclei which cannot be reached with Monte Carlo codes.

The results of these calculations have been benchmarked with the new available data, showing the reliability of the model predictions. These calculations have also been used to estimate the expected production of heavy neutron-rich nuclei in future rare-beam facilities.

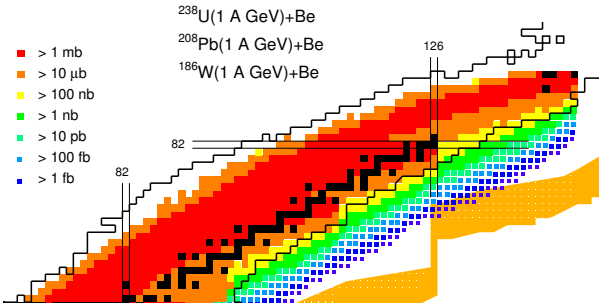

Fig. 2. Estimated production of heavy neutron-rich residues in cold-fragmentation reactions induced by ^{238}U, ^{208}Pb and ^{174}W projectiles at 1 A GeV impinging on a Be target, on top of a chart of the nuclides. The grey scale indicates the maximum production cross section expected from one of the three reactions. The peach coloured area on the lower right side indicates the area of predicted paths for the astrophysical r-process.

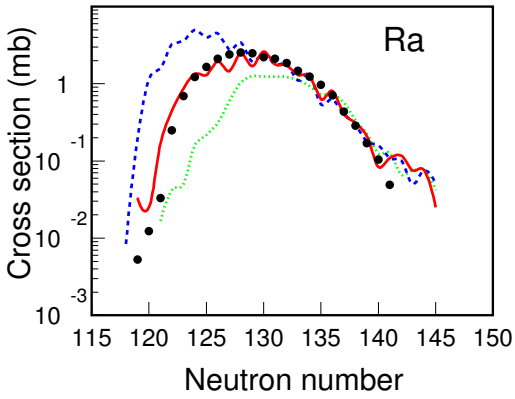

Fig. 3. Production cross sections of Ra isotopes produced in the reaction ^{238}U(1 A GeV)+d compared with model calculations using a Fermi gas level density (dotted line), a level density including ground state shell effects (dashed line) and ground state shell effects and collective excitations (solid line).

Figure 2 shows the calculated production cross sections of heavy neutron-rich nuclei that can be obtained in the fragmentation of ^{238}U, ^{208}Pb and ^{174}W. Great progress is expected in this region of the chart of the nuclides, where the r-process path may even be reached near the waiting point $N = 126$.

3.2 Production of heavy neutron-deficient nuclei

Heavy-exotic nuclei can be produced in fusion-evaporation reactions or by fragmentation(spallation) of heavy nuclei. Both reaction mechanisms lead mainly to the production of neutron-deficient residues and in fact they have been used to extend the proton drip-line up to $Z = 86$ and the 1 μs proton half life line until $Z = 82$. The main difficulty in producing heavier neutron-deficient isotopes is the significant decrease in the survival probability of the compound nucleus due to the fission channel.

Theoretically, survival probability against fission is expected to increase in this region of the chart of the nuclides due to the presence of the neutron shell $N = 126$. However, the measured data show no such increase in the production cross sections of heavy neutron-deficient isotopes around $N = 126$ (see fig. 3). This is thought to be due to a cancellation between shell stabilisation and the enhancement of collective excitations at saddle [16], as discussed in sect. 4.

3.3 Production of medium-mass neutron-rich nuclei

Fission has been widely used to produce medium-mass neutron-rich nuclei to the present frontiers of the nuclide chart [17]. The isotopic distribution of fission-produced residues can be understood in terms of the potential governing this process. The Coulomb term of the nuclear potential is responsible for the neutron excess of the stable fissile nuclei. The asymmetry term preserves the N/Z ratio in the fission process, which results in a large neutron excess in the final residues with respect to the valley of beta stability. Shell effects and fluctuations in the N/Z due to temperature could lead to the production of even more neutron-rich residues.

In order to investigate the fluctuations in N/Z and mass asymmetry induced by the temperature of the fissioning system, several simulations were carried out using the fission code of ref. [18], which again was benchmarked with the new experimental data. Figure 4 represents the distributions of residues after the fission of ^{238}U at different excitation energies in form of a chart of the nuclides. As excitation energy increases, shell effects (double humped distribution) disappear and the fluctuations in mass asymmetry and N/Z increase, populating a greater variety of neutron-rich residues. However, at high excitation energies neutron evaporation sets in, and the residue distribution moves to the neutron-deficient side. These calculations show that for producing the greatest variety of neutron-rich nuclei, the optimum excitation energy of the fissioning system is around 50 MeV.

4 Nuclear structure investigated with spallation reactions

Manifestations of nuclear structure such us even-odd effects or shell closure are known to disappear as the temperature of the nucleus increases. Consequently, signs of nuclear structure are not expected in high-energy reactions such as fragmentation or spallation. However, the accurate measurement of the production yields of residual nuclei in these reactions have revealed complex nuclear-structure phenomena, indicating that the final residual nuclei in high-energy reactions are produced after long evaporation chains of very hot nuclei. The final isotopic composition of the residues then, is determined during the last steps of the evaporation chain, when the nuclei are sufficiently cold and their decay widths are sensitive

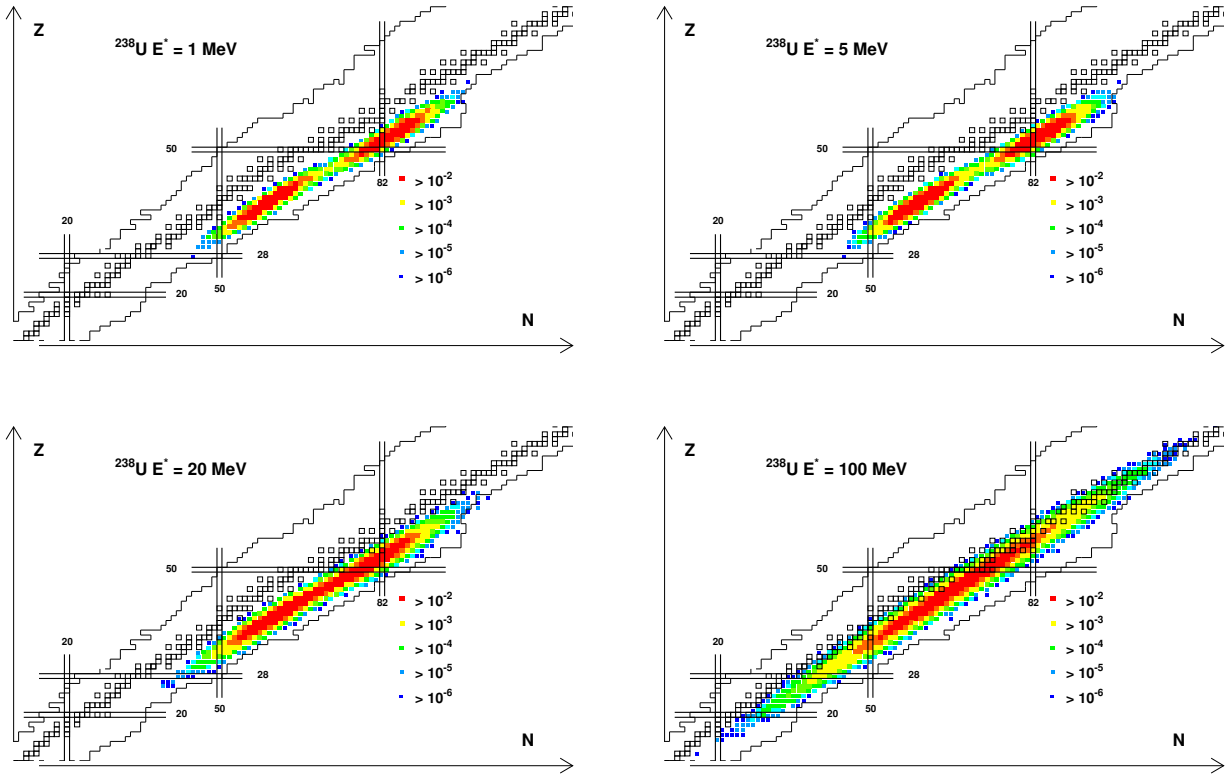

Fig. 4. Relative production yield of residual nuclei after the fission of ^{238}U at different excitation energies above the fission barrier.

to structural effects. Investigation of the production yields from highly-excited nuclei could be a rich source of information about nuclear-structure phenomena in slightly-excited nuclei found at the end of their evaporation process. Two manifestations of nuclear structure, pairing and collective excitations, have been observed in the production yields of spallation and fragmentation residues.

4.1 Even-odd staggering in the production yields of spallation residues

Figure 5 illustrates the production cross sections of light projectile-like residues from the reaction $^{238}\mathrm{U} + \mathrm{Ti}$ at 1 A GeV [19]. The data are sampled according to the neutron excess $N - Z$ for even-mass (left panel) and odd-mass nuclei (right panel), revealing a complex structure. Even-mass nuclei display a clear even-odd effect, which is particularly strong for $N = Z$ nuclei, while odd-mass nuclei show a reversed even-odd effect with enhanced production of odd-Z nuclei, specially those nuclei with larger $N - Z$ values. However, the reversed even-odd effect for nuclei with $N - Z = 1$ vanishes at $Z = 16$, and an enhanced production of even-Z nuclei can again be observed for $Z > 16$. Finally, all observed structural effects seem to vanish as the mass of the fragment increases.

Most of these observations were interpreted using the statistical model framework, including a consistent description of pairing and shell effects in both binding energies and level densities of the parent and daughter nuclei. With odd-mass residues, the even-odd staggering in the production cross sections can be understood as a manifestation of pairing correlations in the particle separation energies. The number of particle-bound states in the final residual nuclei follows the observed staggering in the production yields. However, in describing even-odd staggering in even-mass nuclei, the number of available states in the daughter nucleus along the evaporation chain must be taken into account along with those in the mother nucleus. In both cases and for heavier nuclei, gamma emission becomes a competitive decay channel in the last de-excitation steps, being responsible for the vanishing of the even-odd staggering as mass increases.

In spite of this success, particularly strong staggering observed in the final yields on the $N = Z$ chain could not be reproduced. This is still an unresolved question, but could be due to phenomena such as the Wigner energy, alpha clustering or neutron-proton correlations (see ref. [19] for a detailed discussion).

4.2 Collective excitations in residual nuclei across the shell N = 126

Shell effects also modify binding energies and level densities. As with pairing correlations, they should also appear

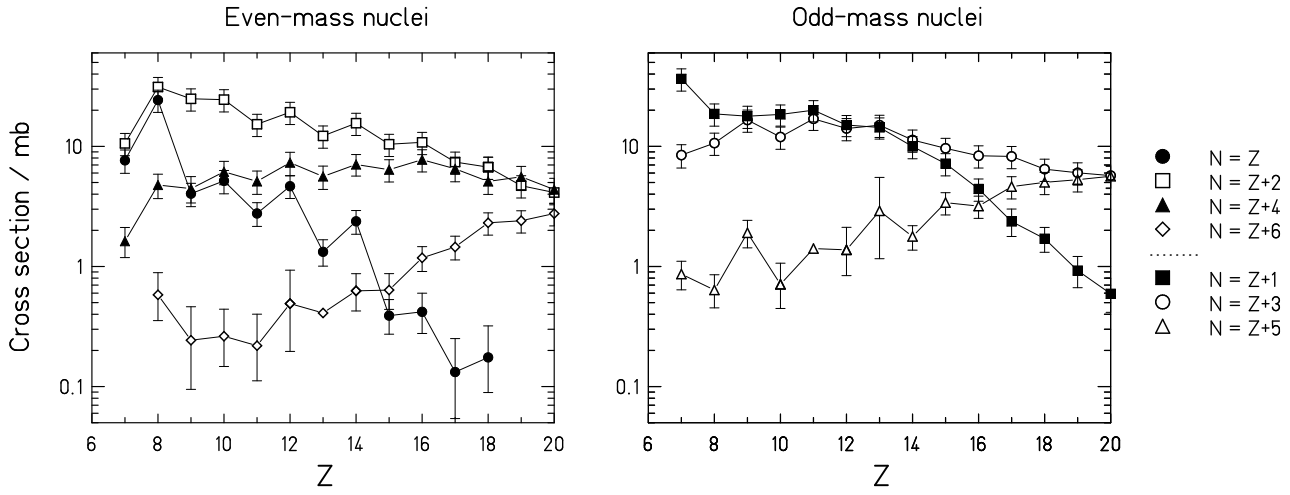

Fig. 5. Formation cross sections of the projectile-like residues from the reaction ^{238}U + Ti, 1 A GeV. The data are given for specific values of $N - Z$. The chain $N = Z$ shows the strongest even-odd effect, while the chain $N - Z = 5$ shows the strongest reversed even-odd effect.

during the last steps of the evaporation chain for nuclei near a shell closure.

The measured production cross sections of residual nuclides in reactions induced by ^{238}U projectiles drew attention to the region of the nuclide chart that crosses the neutron shell $N = 126$, which proved to be very interesting. In this region, the final production cross section of residual nuclei is governed by the competition between neutron or proton evaporation and fission. In fact, the measured cross sections represent the survival probability against fission. Higher fission barriers should lead to an enhanced production cross section of those nuclei (see sect. 3.2). However, no evidence of such an enhancement is observed in the measured cross sections of radium isotopes produced in the reaction ^{238}U(1 A GeV)+d (fig. 3).

Several calculations were carried out using the statistical de-excitation model in an effort to understand these results. The dashed line in fig. 3 indicates the results of calculations that consistently account for shell effects, both in the binding energies and the level densities, while the dotted line represents a calculation where these effects are not accounted for. An enhanced production of radium isotopes around $N = 126$ was clearly predicted by the calculations but not corroborated by the measured data.

The astonishing lack of stabilisation against fission for magic or near magic nuclei was interpreted as an indication of the level-density enhancement due to rotational collective excitations [16]. The large deformation of the mother nucleus at the saddle point favours the appearance of rotational bands above the fission barrier. These collective levels are added to the intrinsic levels of the nucleus, leading to a level density increase at saddle that favours the fission decay channel. The magnitude of this effect compensates for stabilisation against fission due to the presence of shell effects, which modify the binding energy and fission barrier. The solid line in fig. 3 represents a calculation where shell effects are accounted for consistently in both binding energies and level densities, and collective excitation at the saddle point are added to single particle level densities according to ref. [16].

5 Conclusion

The combined use of inverse kinematics with a high-resolution magnetic spectrometer is a powerful technique for investigating spallation reactions, allowing for a precise isotopic identification of all projectile-like residues with a half-life longer than 200 ns. With this technique we could establish the production cross sections with near 10% accuracy.

The large experimental program at GSI enabled us to investigate these reactions using key projectiles that represent different regions of the chart of the nuclides, in particular ^{238}U, ^{208}Pb, ^{136}Xe and ^{56}Fe at energies between 1000 and 300 A MeV. More than 1000 different nuclides were measured and identified for each of these reactions.

The high sensitivity of the residual nuclides final production cross sections to the reaction mechanism provided new and detailed information about the underlying physics of spallation reactions, which has been used to develop and improve model calculations. These reactions models are presently being coupled with complex transport codes to describe the interaction of relativistic projectiles with thick targets. The aim of these calculations is to design target assemblies for neutron production in accelerator driven systems, to be used for nuclear waste transmutation or for the production of non-stable nuclides in future rare-beam facilities. For this purpose, the present data are vital to optimising the production of exotic nuclei in different regions of the chart of the nuclides.

A comprehensive analysis of these results lead us to expect important progress in the production of heavy neutron-rich nuclides, which will result in a considerable expansion of the present limits of the chart of the nuclides.

In contrast, the production of heavy neutron-deficient nuclides will be limited by the extensive depopulation of the final yields due to the fission decay channel. However, fission still remains the optimum reaction mechanism for producing medium-weight neutron-rich isotopes.

Finally, and unexpectedly, spallation reactions can also be a rich source of information to the investigation of nuclear structure. Nuclear structure, specifically, pairing correlations and shell effects, appear in the final yields of residual nuclides produced in these reactions. The challenge ahead is to develop and use theoretical models to quantitatively interpret these results, in order to better understand the complex nuclear-structure behind them.

Most of the results presented in this paper were obtained by a German-French-Spanish collaboration and in particular by P. Armbruster, M. Bernas, A. Boudard, E. Casarejos, T. Enqvist, S. Leray, J. Pereira, F. Rejmund, M.V. Ricciardi, C. Stephan, K.H. Schmidt, J. Taieb and L. Tassan-Got. The work was supported by the following grants EC-Euratom FIKW-CT-2000-00031, MCyT FPA2002-04181-C04-01 and XuGa PGIDIT03PXIC20605PN.

References

1. C.D. Bowman *et al.*, Nucl. Instrum. Methods Phys. Res. A **320**, 336 (1992).
2. C. Rubbia *et al.*, preprint CERN/AT/95-44(ET), 1995.
3. Study Group on Radioactive Nuclear Beams, OECD Megascience Forum, 2000 (`http://www.iupap.org/reports/c12report.html`).
4. NuPECC Report "Radioactive Nuclear Beam Facilities", April 2000.
5. H. Geissel *et al.*, Nucl. Instr. Methods B **70**, 286 (1992).
6. W. Wlazlo *et al.*, Phys. Rev. Lett. **84**, 5736 (2000).
7. J. Benlliure *et al.*, Nucl. Phys. A **683**, 513 (2001).
8. F. Rejmund *et al.*, Nucl. Phys. A **683**, 540 (2001).
9. T. Enqvist *et al.*, Nucl. Phys. A **686**, 481 (2001).
10. `http://www-w2k.gsi.de/charms/data.htm`.
11. J. Taieb *et al.*, Nucl. Phys. A **724**, 413 (2003).
12. M. Bernas *et al.*, Nucl. Phys. A **725**, 213 (2003).
13. E. Casarejos *et al.*, Phys. At. Nuclei **66**, 1413 (2003).
14. J. Pereira *et al.*Nucl. Phys. A **734**, (2004).
15. J. Benlliure *et al.*, Nucl. Phys. A **660**, 87 (1999).
16. A.R. Junghans *et al.*, Nucl. Phys. A **629**, 635 (1998).
17. M. Bernas *et al.*, Phys. Lett. B **415**, 111 (1997).
18. J. Benlliure *et al.*, Nucl. Phys. A **628**, 458 (1998).
19. M.V. Ricciardi *et al.*, Nucl. Phys. A **733**, 299 (2004).